

# Production of C<sub>2</sub>–C<sub>4</sub> Olefins with Fischer-Tropsch-Synthesis: The Effect of Cu Promoter Loading on an Fe–Cu–K/SiO<sub>2</sub> Catalyst

Niko Heikkinen,<sup>\*[a]</sup> Dorela Dhama,<sup>[b]</sup> Ida Uotila,<sup>[a]</sup> Matti Reinikainen,<sup>[a]</sup> and Roland Dittmeyer<sup>[b]</sup>

In this study we focus on the iron-based catalyst to produce C<sub>2</sub>–C<sub>4</sub> olefin hydrocarbons via the high-temperature Fischer-Tropsch synthesis. Promoters have a significant impact on catalyst stability, activity, and product selectivity. Therefore, we investigated the effect of the Cu promoter in an Fe–Cu–K/SiO<sub>2</sub> catalyst. We compared the catalyst without Cu and 1, 2, 3, 4, and 5 wt% Cu loadings. The overall catalyst activity increased from 0 to 3 wt% Cu loading and started to decrease at 4 and 5 wt% Cu loadings. Although overall catalyst activity had an optimum with 3 and 4 wt% Cu loading, the Cu loading had a negligible effect on product selectivity. However, when com-

pared to a non-Cu promoted catalyst, the Cu addition increased the selectivity towards olefinic C<sub>2</sub>–C<sub>4</sub> hydrocarbons. The Fischer-Tropsch experiments were performed in a tubular reactor system at 300 °C, 21 bar and H<sub>2</sub>:CO = 2 at different feed volume flows, with hydrogen activation. According to the performed temperature-programmed dynamic chemisorption analysis, the Cu promoter assisted the iron reduction, and the lower overall activity to 0–2 wt% Cu loading might relate to insufficient dissociated H surface species, rather than the availability of C from dissociated CO.

## Introduction

Recently, interest in renewable and sustainable chemicals has been increasing rapidly. An expanding number of studies have been conducted to understand the surface chemistry of the Fischer-Tropsch to Olefins (FTO) process, with the aim of developing highly efficient iron-based catalysts for the reaction.<sup>[1,2]</sup> There are several reasons for the growing interest, including the increasing annual demand for lower olefins (C<sub>2</sub>–C<sub>4</sub>), finding alternative synthesis routes from syngas (H<sub>2</sub> + CO), and utilizing alternative renewable feedstocks for lower olefin production.<sup>[2]</sup> In this regard, FTO presents an interesting route to supplement and replace energy-intensive lower olefin production from crude oil through steam cracking. In addition, FTO is a compatible technology for renewable resource utilization, when syngas is produced with biomass gasification or from other sustainable CO sources.<sup>[3]</sup> The inherent iron-based catalyst water-gas shift (WGS) reaction is also beneficial when working with

biomass-originating hydrogen-deficient syngas ratios (H<sub>2</sub>/CO ≤ 1), as the ratio can be balanced with the WGS reaction to a suitable range of ~2 for H<sub>2</sub>/CO.<sup>[3–5]</sup>


Olefins are highly reactive and can be converted to many value-added products such as polymers, detergents, adhesives, paper chemicals, and surface modifiers. One example of recent development is the manufacture of renewable polyols and polyurethanes from olefins produced with FTO synthesis.<sup>[6]</sup> Furthermore, lower olefins can be isomerized and oligomerized to high-octane gasoline for road vehicles and aviation.<sup>[7–9]</sup>


The Fischer-Tropsch synthesis (FTS) is a step polymerization, highly exothermic reaction, yielding mainly linear alkanes (Equation 1) and alkenes (Equation 2). The FTO on iron-based catalysts is a structure-sensitive reaction and the catalytic performance strongly depends on the catalyst particle size of the active phase.<sup>[10]</sup> However, limited direct information exists on the effects of the iron particle size on the catalytic performance, mainly because the iron phase composition greatly depends on the iron particle sizes, promoters and supports, and the reported catalysts generally undergo deactivation. During the pre-treatment steps of the iron-based catalysts as well as under real FTO conditions, the carburization process inevitably leads to the formation of a series of iron carbides responsible for the Fischer-Tropsch activity (e.g., ε-Fe<sub>2</sub>C, θ-Fe<sub>3</sub>C and χ-Fe<sub>5</sub>C<sub>2</sub>) and iron oxides facilitating WGS/reverse water-gas shift (RWGS) reaction (e.g., α-Fe<sub>2</sub>O<sub>3</sub>, γ-Fe<sub>2</sub>O<sub>3</sub>, Fe<sub>3</sub>O<sub>4</sub> and FeO),<sup>[4]</sup> significantly increasing the difficulty and complexity in the analysis of iron active phases. Therefore, maintaining a carburized surface and a suitable carbide particle size are the main issues for designing effective iron-based catalysts.<sup>[11]</sup>

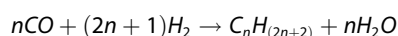
Equation 1

[a] N. Heikkinen, I. Uotila, M. Reinikainen  
VTT Technical Research Centre of Finland, P.O. Box 1000, FIN-02044 VTT,  
Espoo, Finland  
E-mail: niko.heikkinen@vtt.fi

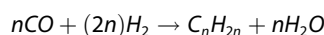
[b] D. Dhama, R. Dittmeyer  
Institute for Micro Process Engineering (IMVT), Karlsruhe Institute of  
Technology (KIT), Hermann-von-Helmholtz-Platz 1, 76344 Eggenstein-Leo-  
poldshafen, Germany

 Supporting information for this article is available on the WWW under  
<https://doi.org/10.1002/cctc.202400560>

 © 2024 The Authors. ChemCatChem published by Wiley-VCH GmbH. This is  
an open access article under the terms of the Creative Commons Attribution  
License, which permits use, distribution and reproduction in any medium,  
provided the original work is properly cited.



Equation 2



To influence the catalyst stability and product selectivity, alkali-promoted iron catalysts have been applied in the industry.<sup>[7]</sup> Many iron-based catalysts have been investigated, and in some cases, they have exhibited high selectivity toward lower olefins when the iron was modified by the addition of promoters.<sup>[12,13]</sup> Despite these promising results, the iron catalysts are mechanically unstable when the reaction is performed at high temperature. Bulk Fe catalysts tend to fragment due to carbon deposition or to density differences between the oxidic and carbide phases present in the working catalyst. Under these conditions, the carbon deposition of the catalysts can block the active sites and induce fragmentation of the catalyst particles.<sup>[14]</sup> Furthermore, localized heating (so-called reaction hot spots) caused by the highly exothermic nature might exist within the catalyst bed, which could threaten the lifetime of the catalyst and the safety of the reactor, if the generated heat cannot be removed effectively. By moving to supported catalysts, the carbon is to a certain degree contained in the pores, iron particles are much smaller, and fragmentation is delayed or does not occur.<sup>[15]</sup>

Several supports have been proposed for the dispersion of the active phase of FTO catalysts, ranging from oxides and molecular sieves to clays and carbonaceous materials. There is consensus that supported Fe catalysts, especially for using SiO<sub>2</sub>, TiO<sub>2</sub>, α-Al<sub>2</sub>O<sub>3</sub>, and nanostructured carbon materials as support, are more suitable for practical applications than unsupported (bulk) Fe catalysts, owing to the higher mechanical stability and dispersion of the active phase.<sup>[4,16]</sup> A strategy to avoid or to restrict the nucleation of carbon deposits on iron-containing particles is to reduce their size from micrometers to nanometers. Small iron nanoparticles do not fragment further upon contact with syngas at high temperatures. If the Fe particles are close together, they tend to aggregate, forming large particles, which ultimately nucleate carbon and fragment.<sup>[16]</sup> The use of a support material increases the stability of iron-based catalysts by serving as a mechanical anchor that maintains the separation of nanoparticles, avoiding the formation of clusters and particle growth.<sup>[4]</sup> However, supports with too strong an interaction may result in iron-support mixed compounds or the forming of active iron carbides. Overly weak iron-support interaction will result in deactivation through active phase sintering or the formation of non-active carbon species.<sup>[14]</sup>

In addition to the support selection and Fe particle control, promoters can be added to the catalyst composition. Cu and K promoters have previously been studied extensively with precipitated catalyst samples; however, less information is available for supported Fe catalysts prepared for instance by incipient wetness impregnation. Furthermore, more information is available on the role of potassium.<sup>[17–20]</sup> The first insight with a Cu-promoted iron-based catalyst was that adding Cu led to an

increased rate of reduction, enabling a lower reduction temperature.<sup>[8]</sup> Many studies reported an increase in FTS and WGS activity, when adding Cu as a promoter.<sup>[21–28]</sup> Bukur et al.<sup>[19]</sup> also showed that increased activity is independent of K loading, whereas selectivity is strongly dependent on K loading. Compared to non-promoted and K-promoted catalyst samples, the Cu-promoted catalyst had the highest reaction rate, while K promotion (0.2–1 wt%) resulted in increased heavy hydrocarbon selectivity. In addition to the suppressed olefin hydrogenation and isomerization reactions, the Fe–K catalyst presented iron reduction inhibition. This inhibition was counterbalanced with an addition of Cu, enhancing the iron carbide formation. A similar finding was presented by Chernavskii et al.<sup>[18]</sup> with an SiO<sub>2</sub> supported Fe–Cu–K catalyst. They reported enhanced iron dispersion, an increased reaction rate related to Cu promoter, and K affecting mainly the selectivity rather than the reaction rate. The Cu promoter increased activity due to the enhanced reduction of hematite to magnetite and assisted direct hematite carbidisation to Hägg iron carbide. Potassium promoter also increased the catalyst activity when compared to non-promoted catalyst, but the decreased hematite reduction limited the iron carbide phase formation and the resulting catalyst activity. The effect of potassium on hydrocarbon selectivity was assumed to result from an altered electronic interaction between the iron carbide and potassium. A similar assumption was reached by Cano et al.,<sup>[29]</sup> who showed through density functional theory (DFT) calculations that Cu- and K-promoted Fe on SBA-15 catalyst modifies the electronic density distribution, promoting electronic transfer towards the Fe atoms. As a result, secondary olefin hydrogenation is suppressed and the chain growth probability is increased.<sup>[18,20,29]</sup>

O'Brien and Davis<sup>[22]</sup> investigated the impact of Cu promoter, testing three iron catalysts with Cu loadings from 0 to 2 atomic ratio per 100 Fe. Cu increased the rate of FTS and WGS reactions, while having no effect on CO<sub>2</sub> selectivity. Furthermore, increasing the Cu loading led to decreased methane and increased C<sub>11+</sub> hydrocarbon selectivity, while having negligible impact on the alkene selectivity.

The Fischer-Tropsch reaction and catalyst undergo four phases: a) reduction of the catalyst, b) reagent gas adsorption and surface reactions, c) intermediate formation, and d) desorption and chain growth. Table 1 summarizes these four reaction phases and key findings in the literature on the role of Cu- and K-promoters. Generally, Cu seems to increase the catalyst's overall activity; however, there are controversial outcomes with respect to its impact on the selectivity. Some studies propose that Cu affects only the catalyst activity, without a significant effect on selectivity.<sup>[25–27,30]</sup> Other studies report a slight increase in C<sub>5+</sub> selectivity.<sup>[19,24,28,31]</sup> Some studies focusing on light olefins report only minute changes to the C<sub>2</sub>–C<sub>4</sub> selectivity when Cu loading varied.<sup>[25,26,30]</sup> Other studies report decreasing olefin yield as a function of increasing Cu loading<sup>[19,27,28]</sup> while others report an increase in the olefin share upon increasing Cu loading.<sup>[24,31]</sup>

In this work we focus on the effect of Cu loading on the FTO reaction. With six catalysts, we address the effect of Cu on

| Reaction phase/<br>Promoter | a) Reduction   | b) Adsorption and surface reactions  | c) Intermediate formation   | d) Desorption and chain growth  |
|-----------------------------|--|--|---|---|
| Cu                          | Assists hematite reduction by enhanced hydrogen dissociation <sup>[4,5,18]</sup><br>Increases Fe dispersion <sup>[4,5,18]</sup>  | Decreases adsorption strength for CO <sup>∗</sup> <sup>[5,32]</sup><br>Enhances H-assisted CO dissociation route <sup>[5,32]</sup><br>Assists carbide (active phase) formation by suppressing iron-support interactions <sup>[4,5]</sup><br>Increases water-gas shift (WGS) activity <sup>[4,19]</sup> | Decreases adsorption strength for CH-intermediates <sup>[32]</sup>  | Decreases chain growth probability <sup>[4,5,18,32]</sup>   |
| K                           | Inhibits Fe <sub>2</sub> O <sub>3</sub> reduction to Fe <sub>3</sub> O <sub>4</sub> <sup>[18]</sup><br>Assists Fe <sub>3</sub> O <sub>4</sub> carbidization <sup>[18]</sup><br>Increases Fe dispersion <sup>[18]</sup> | Enhances overall CO dissociation through alkali metal electron donation properties, weakening C–O bonds <sup>[18]</sup><br>Increases water-gas shift (WGS) activity <sup>[4,19]</sup>  | Decreases methane formation <sup>[5]</sup><br>Promotes olefin formation through decreased hydrogenation activity <sup>[5,18,19]</sup> | Increases formation rate of heavy hydrocarbons <sup>[5,18,19]</sup><br>Promotes chain growth probability <sup>[5,18,19]</sup> |

the catalyst activity and selectivity with varying nominal Cu loading of 0, 1, 2, 3, 4, 5 wt%. The main Fischer-Tropsch synthesis experimental work was carried out using a tubular reactor. Additional experiments were carried out with 1% and 3% Cu loading in an annular gap reactor. The description of the annular gap experimental setup and the results are presented in the supplementary material.

## Results and Discussion

### Catalyst Characterization

The results for sorption measurements are shown in Table 2. The specific surface area and pore volume decreased slightly as a function of Cu loading, whereas the pore diameter remained the same with all catalyst samples.

Figure 1 presents the H<sub>2</sub>- and CO-TPD results for all samples. In the CO-TPD measurement, the total CO uptake was 12, 40, 40, 40, 26, and 28 μmol/g<sub>cat</sub> for Cu-0%, Cu-1%, Cu-2%, Cu-3%, Cu-4%, and Cu-5% samples, respectively (see Table 2). The CO profiles have two desorption regions: low (100–300 °C) and high (400–700 °C). Low temperature CO desorption is assigned to weak metal oxide adsorption, while the high temperature region is related to dissociated surface species.<sup>[32]</sup> In the H<sub>2</sub>-TPD analysis, the desorption peak at 500 °C is related to dissociated hydrogen species. The response for the dissociated hydrogen

increases with increasing Cu loading. In agreement with Wan et al.<sup>[33]</sup> Cu loading increases the dissociated H<sub>2</sub> surface species. In the CO-TPD measurement, the fraction of dissociated CO adsorption with respect to weak CO adsorption are presented at Table 2. The ratio of dissociated CO and weak CO was determined by integrating the CO-TPD peak area and dividing the dissociated CO peak area by the weak CO peak area. The ratio of CO desorption peaks remained similar with 2–5 wt% Cu loading, while the Cu-1% sample had increased fraction of dissociated CO. According to literature, CO adsorbs preferentially on iron rather than on copper.<sup>[33–35]</sup> The increase of copper content generally lowers the dissociated CO adsorption volume (see Table 2). However, it is not clear why in our experiments the catalyst without Cu had rather low total CO adsorption capacity compared to samples with Cu.<sup>[33,35]</sup>

Catalyst reduction behavior was investigated with H<sub>2</sub> temperature programmed reduction (H<sub>2</sub>-TPR). Figure 2 presents the TPR results with two reduction temperature ranges. The first region at 150–350 °C is related to CuO and α-Fe<sub>2</sub>O<sub>3</sub> reduction to Cu and FeO/Fe<sub>3</sub>O<sub>4</sub>, respectively. The second region at 350–650 °C corresponds to the terminal reduction to Fe.<sup>[18,32]</sup> According to Figure 2, Cu promoter assisted the iron reduction. Interestingly, the first reduction peak temperature decreases from Cu-0% to Cu-3% sample and increases again with Cu-4% and Cu-5%. Similar behavior can be seen in the high temperature range, where terminal iron reduction is lowest for 3% Cu and is increased with all other samples.

| Sample  | Cu-0% | Cu-1% | Cu-2% | Cu-3% | Cu-4% | Cu-5% |
|---|-------|-------|-------|-------|-------|-------|
| BET surface area (m <sup>2</sup> g <sup>-1</sup> ) <sup>a</sup>     | 200   | 197   | 196   | 194   | 192   | 190   |
| Pore volume (cm <sup>3</sup> g <sup>-1</sup> ) <sup>a</sup>         | 0.74  | 0.74  | 0.73  | 0.72  | 0.71  | 0.70  |
| Pore diameter (nm) <sup>a</sup>                                     | 14.9  | 15.1  | 14.7  | 14.9  | 14.8  | 14.7  |
| Total CO uptake (μmol g <sub>cat</sub> <sup>-1</sup> ) <sup>b</sup> | 12    | 40    | 40    | 40    | 26    | 28    |
| Weak CO adsorption (μmol g <sub>cat</sub> <sup>-1</sup> )           | 3.5   | 10.0  | 14.0  | 14.4  | 9.4   | 9.5   |
| Dissociated CO adsorption (μmol g <sub>cat</sub> <sup>-1</sup> )    | 8.5   | 30.0  | 26.0  | 25.6  | 16.6  | 18.5  |
| Fraction of dissociated CO adsorption (%)                           | 71%   | 75%   | 65%   | 64%   | 64%   | 66%   |

<sup>a</sup> N<sub>2</sub> sorption measurement results, <sup>b</sup> CO temperature programmed desorption (CO-TPD) measurement results.

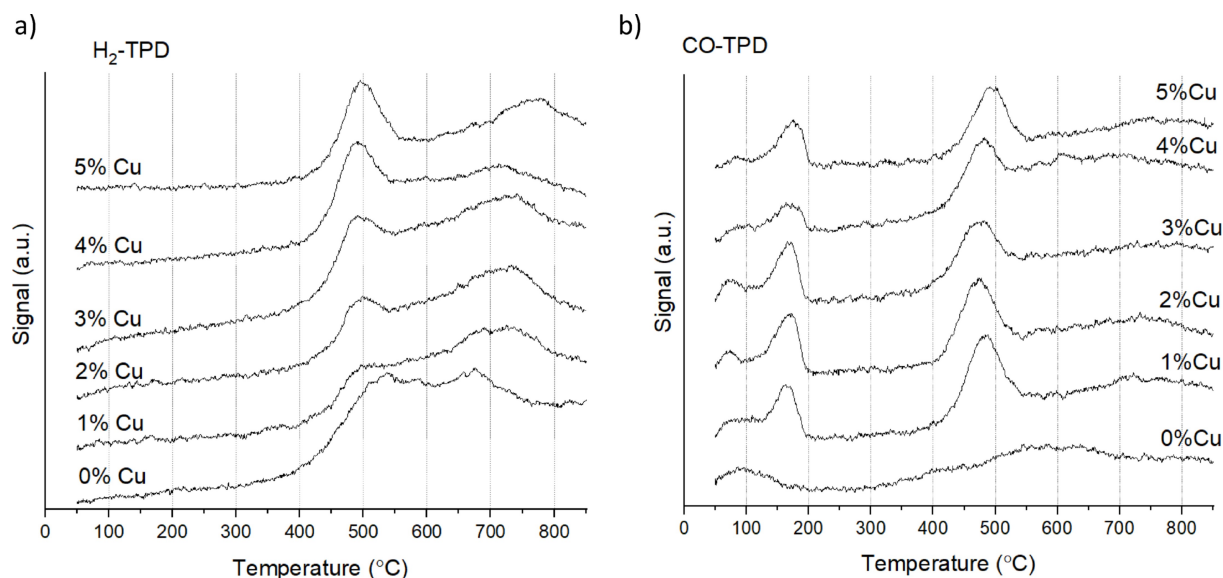


Figure 1. a) H<sub>2</sub>- and b) CO-TPD profiles of the reduced catalysts with varying Cu loading.

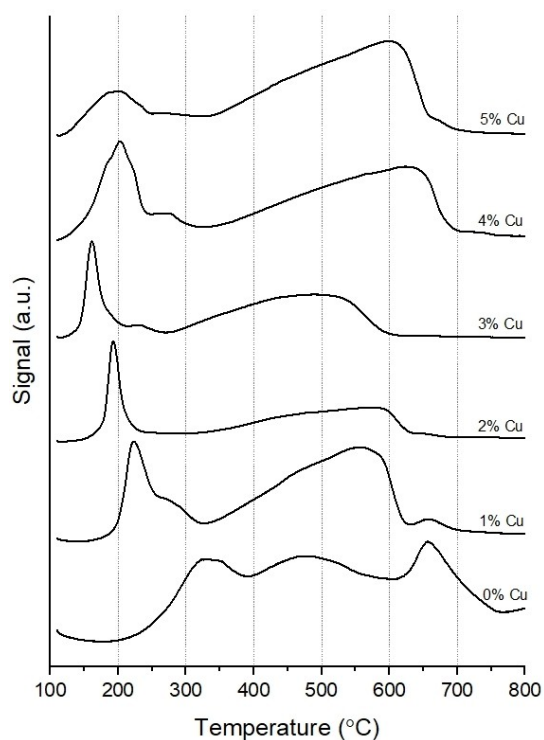


Figure 2. H<sub>2</sub>-TPR profiles of the reduced catalysts with varying Cu loading.

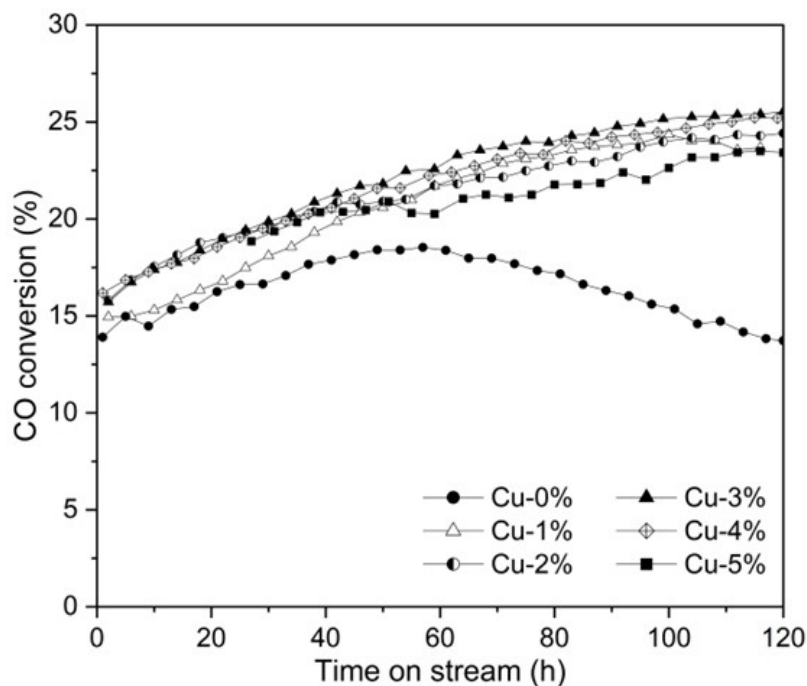
### Effect of Cu Loading on the Catalyst Activity

Figure 3 presents CO conversion for all catalyst samples from the first 120 h time-on-stream (first reaction flow setpoint). The Cu-0% catalyst showed increased CO conversion until 50–60 h, whereas with Cu promoted samples, the CO conversion increased until 120 h. With the unpromoted Fe-catalyst, after 50–60 h time-on-stream (TOS), the CO conversion started to decrease. The decrease in the CO conversion was assumed to

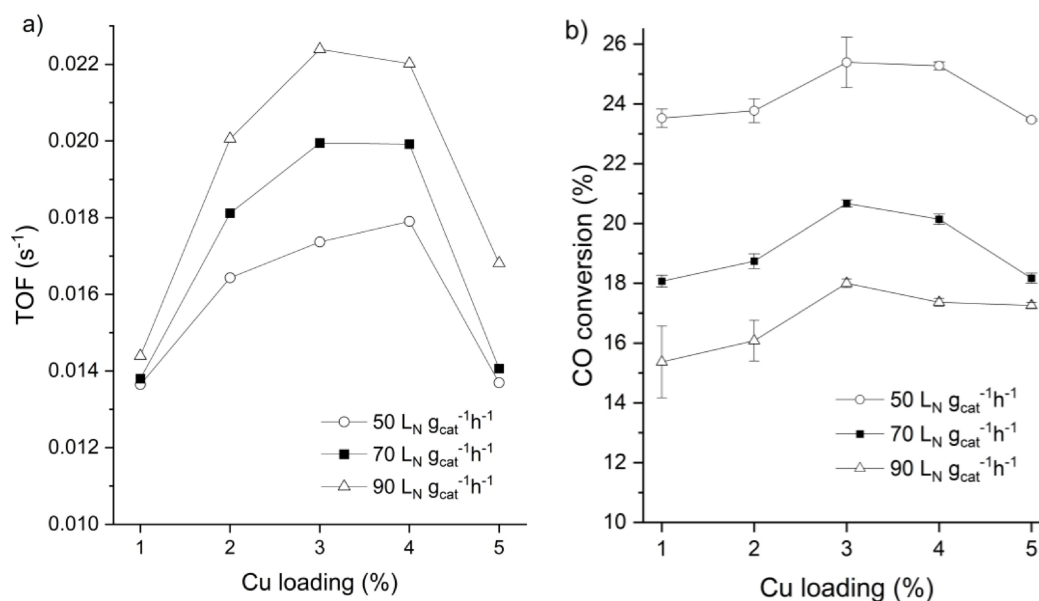
relate to deactivation, where the mechanism may relate to increased coking as the hydrogen adsorption without Cu is remarkably lower than with the promoted catalysts.<sup>[36,37]</sup> The stability and activity of the catalyst improved significantly with the addition of Cu promoter. Gong et al.<sup>[32]</sup> have presented that a Cu promoter decreases the basicity of the catalyst surface and changes the metal-support interaction, leading to an inhibited rate of deactivation.

Figure 4 presents the turnover frequency (TOF) and the Cu-promoted catalyst activity from three different conversion levels (varied by the total gas flow). From the point where the CO conversion was stabilized, the turnover frequency was calculated as moles of CO converted per second per moles of iron in the catalyst. The molar amount of iron was calculated based on the inductively coupled plasma optical emission spectroscopy (ICP-OES) analysis results. As shown in Figure 4 the highest activity was attained with 3 and 4 wt% Cu loadings, where low (< 3 wt%) Cu loading and high (> 4 wt%) resulted in decreased turnover frequency and CO conversion.

The catalytic activity results in Figure 4 seem to correlate with the H<sub>2</sub>- and CO-TPD measurement results (see Figure 1). According to the H<sub>2</sub>-TPD results, the dissociated H<sub>2</sub> species increased with increasing Cu loading. Then, the Cu-1% sample has less dissociated H on the surface for the Fischer-Tropsch reaction. Furthermore, the ratio of dissociated CO and weakly adsorbed CO for the Cu-1% was higher than other Cu loadings. It was assumed that the overall lower Cu-1% catalyst activity was mainly due to the insufficient pool of H surface species, rather than the availability of C from dissociated CO. In addition to the TPD measurements, the general trend in the TPR measurements (see Figure 2) are similar to the catalytic activity in Figure 4. According to our results, 1–2 wt% Cu enhances the catalyst reducibility, resulting in an increased overall activity, 3–4 wt% Cu is the optimum loading, and 5 wt% Cu loading begins to resist reduction and decreases the overall activity.



**Figure 3.** CO conversions for Fe–Cu–K/SiO<sub>2</sub> catalysts with 0–5 wt% Cu promoter over time-on-stream under reaction conditions of 300 °C, 21 bar, H<sub>2</sub>/CO = 2 and GHSV of 50 L<sub>N</sub> g<sub>cat</sub><sup>-1</sup> h<sup>-1</sup> (L<sub>N</sub> meaning Norm Liter). The CO conversion over time-on-stream for all the tested gas hourly space velocities can be found in the Supplementary material (Figure A4).



**Figure 4.** a) Turnover frequency (TOF) and b) CO conversion as a function of catalyst Cu loading in different gas hourly space velocities during 120–170 h time-on-stream.

In comparison to other relevant research work, Peña et al.<sup>[4]</sup> studied the effect of Cu content on the formation of the active Hägg carbide with varying Cu loading of 0.6, 2.0 and 5.0 wt% on a supported 15 wt% Fe/Al<sub>2</sub>O<sub>3</sub> catalyst. They reported that iron carbide formation did not significantly increase upon increasing Cu loading from 2 to 5 wt%. Their observation is similar to our reported catalyst activity in Figure 4, where the

catalytic activity was highest with 3–4 wt% samples. Our results are also in agreement with the work of O'Brien et al.,<sup>[22]</sup> where they showed that the catalyst activity increased when increasing the Cu loading on a precipitated 100Fe/4.6Si/Cu/1.4 K catalyst from 0.1 to 2 Cu in atomic ratio (corresponding to ~0.1 to 2.2 wt% of Cu). With a low Cu loading on a precipitated Fe-catalyst, Li et al.<sup>[25]</sup> reported that the catalyst activity remained

unchanged when increasing the atomic Cu/Fe ratio from 0.01 to 0.02 in a Fe<sub>2</sub>O<sub>3</sub>-ZnO-K-Cu catalyst (corresponding to 0.2 to 0.4 wt% of Cu).

### Effect of Cu Loading on Catalyst Selectivity

Figure 5 presents hydrocarbon (HC) selectivity for all catalyst samples. The selectivity and CO conversion values are reported at a pseudo-steady state, for Cu-0% catalyst at ~55 h time-on-stream, gas hourly space velocity (GHSV) of 50 L<sub>N</sub>/g<sub>cat</sub>h, and Cu promoted catalysts ~145 h time-on-stream, GHSV of 70 L<sub>N</sub>/g<sub>cat</sub>h. The Cu-0% catalyst had higher methane selectivity (35.5%) when compared to the Cu-promoted catalysts with methane selectivity at ~26%. The presence of Cu increased light olefin and C<sub>5+</sub> selectivity. Similar findings have been reported by others, where K- and Cu-promoted Fe catalysts showed an increased olefin to paraffin ratio for the C<sub>2</sub>-C<sub>4</sub> hydrocarbons.<sup>[25,30]</sup> In our experiments, the amount of Cu loading had a negligible effect on hydrocarbon product selectivity. Selectivity to CO<sub>2</sub> was around 27–29% for all the samples under the used reaction conditions.

Hydrocarbon product selectivity as a function of CO conversion is presented in Figure 6. CO<sub>2</sub> is omitted from the hydrocarbon selectivity values. The results are obtained from a similar CO conversion level, as the conversion influences the selectivity. Interestingly, increasing the amount of Cu promoter from 1 wt% to 5 wt% did not have a significant effect on the product selectivity at a similar conversion level. Furthermore, the increase in the CO conversion did not have a clear effect on the selectivity of methane or heavier hydrocarbons. The C<sub>5+</sub> selectivity increased slightly for Cu-1%, Cu-2%, and Cu-3%

catalysts as the conversion increased. The C<sub>5+</sub> selectivity was 35–38% and methane selectivity 25–26.5% over the experimented CO conversions. The increased CO conversion decreased C<sub>2</sub>-C<sub>4</sub> olefin selectivity and C<sub>2</sub>-C<sub>4</sub> olefin to paraffin ratio. The C<sub>2</sub>-C<sub>4</sub> olefin selectivity of the Cu-promoted iron catalysts was around 27–30% and the C<sub>2</sub>-C<sub>4</sub> olefin to paraffin ratio was 2.8–3.4. The Cu-4% catalyst had a slightly improved C<sub>2</sub>-C<sub>4</sub> olefin to paraffin ratio compared to other catalysts, with Cu loadings of 1, 2, 3, and 5 wt%.

### Conclusions

The effect of Cu promoter on Fischer-Tropsch to C<sub>2</sub>-C<sub>4</sub> olefins performance was investigated with six Fe-Cu-K/SiO<sub>2</sub> catalysts having Cu loadings of 0, 1, 2, 3, 4 and 5 wt%. The Fischer-Tropsch experiment results showed that adding Cu to a supported iron-based catalyst improved the activity and stability of the catalyst. The results from CO-TPD showed that the presence of Cu had only a minor effect on the CO adsorption and desorption characteristics. H<sub>2</sub>-TPD indicated that increasing Cu loading resulted in an increased amount of dissociated H species on the catalyst surface. The H<sub>2</sub>-TPR results showed that the presence of Cu promoter decreased the reduction temperature of iron oxide with the lowest reduction temperature related to 3 wt% Cu catalyst. With respect to selectivity, the presence of Cu decreased CH<sub>4</sub>, increased C<sub>2</sub>-C<sub>4</sub> olefin, and increased C<sub>5+</sub> hydrocarbon selectivity compared to the catalyst without the Cu promoter. However, hydrocarbon selectivity was barely affected by the amount of Cu loading between 1 to 5 wt%, while a slight improvement in the overall activity was observed with 3 and 4 wt% Cu catalysts.

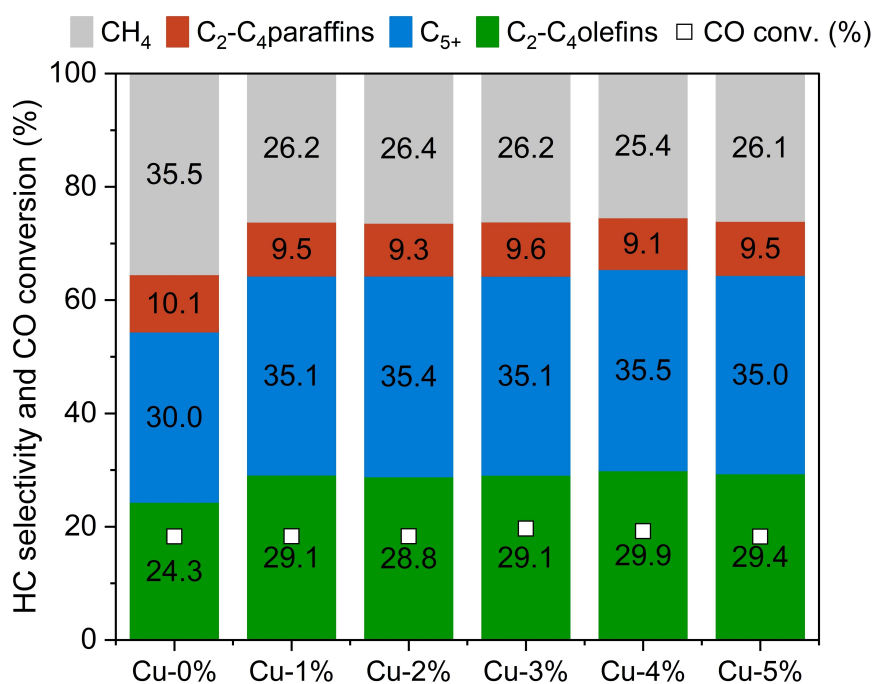


**Figure 5.** Catalytic performance of 0–5 wt% Cu catalysts with tubular reactor at around the same CO conversion level. Reaction conditions: 21 bar, 300 °C, H<sub>2</sub>/CO = 2. The CO<sub>2</sub> is excluded from the hydrocarbon selectivity values.

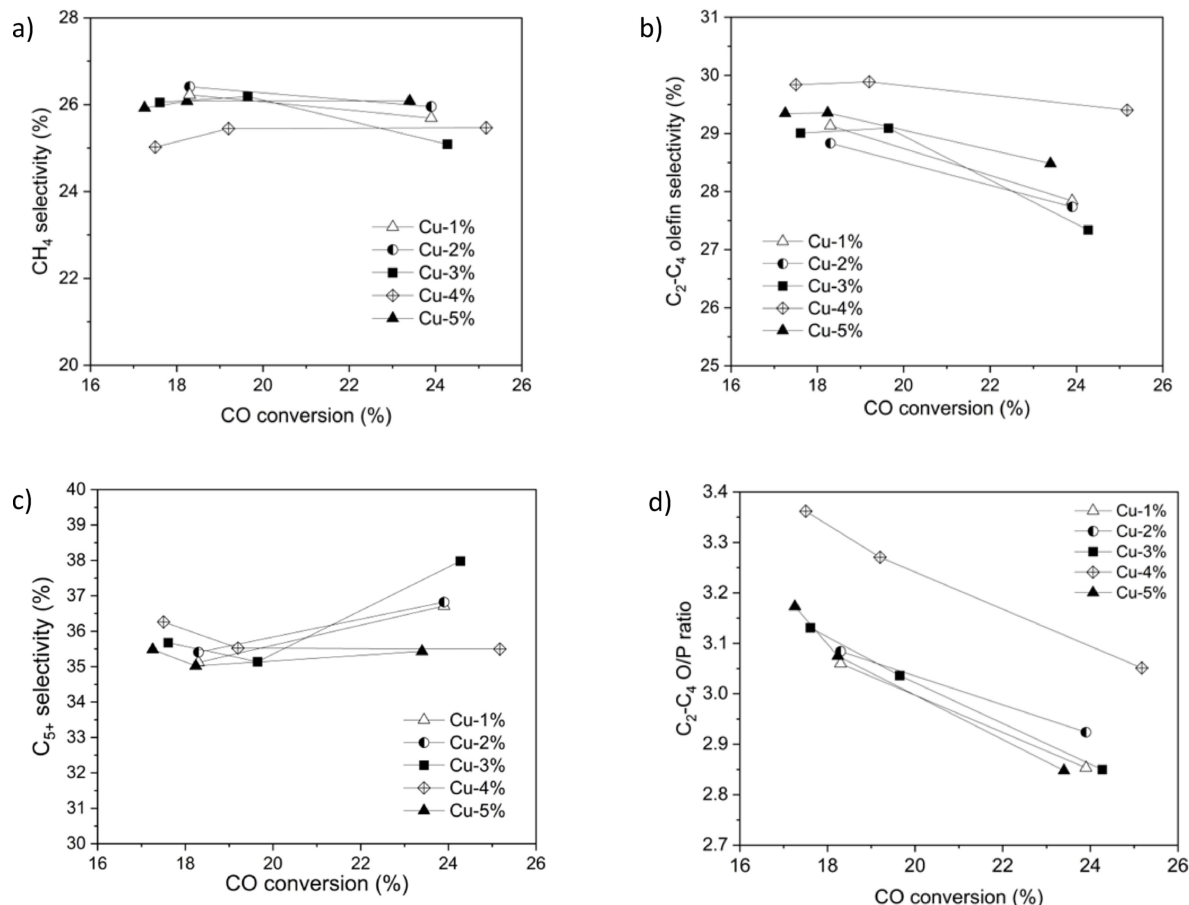


**Figure 6.** Hydrocarbon selectivity over CO conversion for catalysts with 1–5 wt % Cu. a) CH<sub>4</sub> selectivity b) C<sub>2</sub>–C<sub>4</sub> olefin selectivity, c) C<sub>5</sub>+ selectivity and d) C<sub>2</sub>–C<sub>4</sub> olefin to paraffin ratio over the tested CO conversion range.

## Experimental

### Catalyst Preparation

Five SiO<sub>2</sub>-supported iron-copper-potassium catalysts with different copper loadings were prepared by two-step incipient wetness impregnation. In addition, one catalyst was prepared with the same Fe and K loadings and without Cu. Two-step impregnation was used to ensure complete precursor dissolution into water solvent. For the prepared catalysts, Fe and K loadings were constant and only Cu loading was varying with 0, 1, 2, 3, 4, and 5 wt%. The following notation was given for the catalysts: Cu-0%, Cu-1%, Cu-2%, Cu-3%, Cu-4%, and Cu-5%. Fe, Cu, and K loadings are reported

as a weight fraction with respect to the mass of SiO<sub>2</sub> support. Table 3 presents target loadings for each active component and corresponding loadings measured using ICP-OES.

Prior to the catalyst preparation, the catalyst support (Saint-Gobain NordPro SS6\*138) was crushed and sieved to 100–200 μm and dried under vacuum for 1 h. Catalyst precursors Fe(NO<sub>3</sub>)<sub>3</sub>·9H<sub>2</sub>O (Merck, 99.0%), Cu(NO<sub>3</sub>)<sub>2</sub>·3H<sub>2</sub>O (Sigma–Aldrich, 99.0%), and KNO<sub>3</sub> (Merck, 99.0%) were dissolved in deionized water and carefully added to the catalyst support. After 1 h of absorption, the catalyst was dried at 80 °C under a vacuum for 4 h. After the first impregnation step, the second impregnation was performed in the

**Table 3.** Catalyst preparation target loadings for each component and ICP-OES analysis results for Fe, Cu, and K loadings for the prepared catalyst samples.

| Element                            | Cu-0%   | Cu-1% | Cu-2% | Cu-3% | Cu-4% | Cu-5% |
|------------------------------------|---------|-------|-------|-------|-------|-------|
| <b>Target loading</b>              |         |       |       |       |       |       |
| Fe loading (wt%)                   | 16.5    | 16.5  | 16.5  | 16.5  | 16.6  | 16.7  |
| Cu loading (wt%)                   | 0.0     | 0.9   | 1.8   | 2.7   | 3.6   | 4.5   |
| K loading (wt%)                    | 0.4     | 0.4   | 0.4   | 0.4   | 0.4   | 0.4   |
| <b>ICP-OES measurement results</b> |         |       |       |       |       |       |
| Fe loading (wt%)                   | 15.4    | 15.5  | 15.0  | 15.0  | 14.6  | 15.2  |
| Cu loading (wt%)                   | < 0.003 | 1.2   | 2.2   | 3.0   | 3.7   | 4.7   |
| K loading (wt%)                    | 0.6     | 0.5   | 0.5   | 0.5   | 0.5   | 0.4   |

same way, without the last drying step. Instead, catalyst calcination was done in a quartz tube rotavapor in air flow at 400 °C for 4 h.

### Catalyst Characterization

Catalyst sorption measurements were all conducted in a Micromeritics 3Flex instrument. The catalyst reducibility was studied by temperature-programmed reduction H<sub>2</sub>-TPR. In H<sub>2</sub>-TPR, the sample was preheated in a 65 mL/h He flow to 250 °C with 5 °C/min ramp and then cooled down to 40 °C with the same temperature ramp, to remove water from the sample. After cooling down, the gas was changed to H<sub>2</sub> and the reduction temperature program was started. The sample was heated to 750 °C with a 2 °C/min temperature ramp and kept at this temperature for 4 h. The TPR analysis had ~1 g and TPD ~400 mg of sample loaded into a u-shaped quartz analysis tube. The CO uptake in the CO-TPD measurement was determined from the known pulsed volume during the CO adsorption. Typically, 3–4 adsorption pulses were required to saturate the catalyst sample with CO. The CO response was measured with a thermal conductivity detector after the u-shaped quartz analysis tube. In the TPD measurement, the temperature was increased from 50 °C to 900 °C with a ramp rate of 10 °C/min. In H<sub>2</sub>-TPD, the sample was first pre-treated under H<sub>2</sub> flow at 350 °C for 3 hours and then cooled down to 50 °C. Subsequently, the sample was treated under H<sub>2</sub> flow for 90 min and then purged with He flow for 1 h. After that, temperature was increased to 900 °C with 10 °C/min heating rate for the H<sub>2</sub>-TPD measurement. N<sub>2</sub> physisorption was used to determine the Brunauer-Emmett-Teller (BET) surface area (m<sup>2</sup>/g), pore volume (ml/g), and pore diameter (nm) for the SiO<sub>2</sub> support and catalyst samples. A catalyst sample (~100 mg) was degassed for 12 h at 200 °C prior to the analysis.

Fe, Cu, and K loadings were measured with ICP-OES (5110 SVDV, Agilent Technologies). Prior to the analysis, samples (~20–25 mg) were digested with microwave-assisted acid digestion in the presence of HNO<sub>3</sub>, HF, H<sub>2</sub>SO<sub>4</sub>, and H<sub>3</sub>PO<sub>4</sub>. After complete digestion, samples were diluted in ratios of 1:5 and 1:10 for the OES measurement. Multi-elemental solutions (Inorganic Ventures) were used as standards and control samples in the ICP-OES analysis. Measurement uncertainty of the ICP-OES analysis was 10%.

### Experimental Setup and Experimental Procedure

The Fischer-Tropsch synthesis for catalysts with 0–5 wt% Cu loading was conducted in a fixed-bed Hastelloy tubular reactor (i.d. of 9.1 mm). For each test, a catalyst with a weight of 0.2 g was diluted with 3 g of SiC (particle size 105 μm) before loading to the reactor. The reactor tube was heated in a furnace and the temperature of the catalyst bed was monitored with K-type thermoelement. A wax trap was placed after the reactor outlet to collect the heavy hydrocarbon products. The reactor system was placed inside a hotbox at 160 °C to control the temperature and to preheat the reactor inlet lines. The outlet gas was then directed to a liquid-liquid-gas separator (LLG) placed outside the hotbox and cooled down to 5 °C. The liquid products were condensed in LLG and collected for offline analysis (Shimadzu GC-2030). The catalyst was reduced prior to the reaction at 350 °C, at atmospheric pressure and in a flow of 60 ml/min H<sub>2</sub> + 40 ml/min N<sub>2</sub> overnight (17 h). After the reduction temperature was cooled down to 300 °C and the reactor was pressurized to 21 bar<sub>a</sub>. The flow rate of feed gas H<sub>2</sub>, CO, and internal standard 10 vol.% of N<sub>2</sub> was adjusted with mass flow controllers (Bronkhorst). The reaction outlet gas was analyzed by an online gas chromatograph (Shimadzu GC-2030) with an Rt-Q-Bond column connected to flame ionization detector (FID) to analyze hydrocarbon products and Porapak Q+Carboxen-1000 column with thermal conductivity detector (TCD) for analysis of H<sub>2</sub>, N<sub>2</sub>, CO,

CH<sub>4</sub>, and CO<sub>2</sub>. The reaction conditions of the Fischer-Tropsch synthesis were  $T=300\text{ }^{\circ}\text{C}$ ,  $P=21\text{ bar}_a$  and H<sub>2</sub>/CO with a ratio of 2 while testing three different gas hourly space velocities (GHSV) of 50, 70, and 90 L<sub>N</sub>g<sub>cat</sub><sup>-1</sup>h<sup>-1</sup>. After starting the reaction, the 1–5 wt% Cu loaded catalysts activated during the first 110 hours until the reaction stabilized. The first setpoint was carried on for around 120 h and each setpoint was run for at least 12 hours.

### Conflict of Interests

The authors declare no conflict of interest.

### Data Availability Statement

Data sharing is not applicable to this article as no new data were created or analyzed in this study.

- [1] J. Sun, Y. Chen, J. Chen, *Catal. Commun.* **2017**, *91*, 34–37.
- [2] H. M. Torres Galvis, K. P. De Jong, *ACS Catal.* **2013**, *3*, DOI 10.1021/cs4003436.
- [3] G. Liu, E. D. Larson, R. H. Williams, T. G. Kreutz, X. Guo, *Energy Fuels* **2011**, *25*, 415–437.
- [4] D. Peña, L. Jensen, A. Cognigni, R. Myrstad, T. Neumayer, W. van Beek, M. Rønning, *ChemCatChem* **2018**, *10*, 1300–1312.
- [5] V. R. R. Pendyala, G. Jacobs, M. K. Gnanamani, Y. Hu, A. MacLennan, B. H. Davis, *Appl Catal A Gen* **2015**, *495*, 45–53.
- [6] BECCU project. www.beccu.fi. Accessed 15 February 2024., "BECCU. www.beccu.fi. Accessed 15 February 2024." **Business Finland**.
- [7] V. U. S. Rao, G. J. Stiegel, G. J. Cinquegrane, R. D. Srivastava, *Fuel Process. Technol.* **1992**, *30*, 83–107.
- [8] M. E. Dry, in *Handbook of Heterogeneous Catalysis*, Wiley, **2008**.
- [9] R. B. Anderson, *Catalysis* **1956**, *4*, 29–255.
- [10] H. M. Torres Galvis, J. H. Bitter, T. Davidian, M. Ruitenbeek, A. I. Dugulan, K. P. De Jong, *J. Am. Chem. Soc.* **2012**, *134*, DOI 10.1021/ja304958u.
- [11] D. Wang, B. Chen, X. Duan, D. Chen, X. Zhou, *J. Energy Chem.* **2016**, *25*, 911–916.
- [12] W. Ngantsoue-Hoc, Y. Zhang, R. J. O'Brien, M. Luo, B. H. Davis, *Appl Catal A Gen* **2002**, *236*, 77–89.
- [13] K. Cheng, V. V. Ordonsky, B. Legras, M. Virginie, S. Paul, Y. Wang, A. Y. Khodakov, *Appl Catal A Gen* **2015**, *502*, 204–214.
- [14] E. de Smit, B. M. Weckhuysen, *Chem. Soc. Rev.* **2008**, *37*, 2758.
- [15] K. Keyvanloo, M. K. Mardkhe, T. M. Alam, C. H. Bartholomew, B. F. Woodfield, W. C. Hecker, *ACS Catal.* **2014**, *4*, DOI 10.1021/cs401242d.
- [16] K. Cheng, M. Virginie, V. V. Ordonsky, C. Cordier, P. A. Chernavskii, M. I. Ivantsov, S. Paul, Y. Wang, A. Y. Khodakov, *J. Catal.* **2015**, *328*, 139–150.
- [17] Gavrilović, Save, Blekkan, *Catalysts* **2019**, *9*, 351.
- [18] P. A. Chernavskii, V. O. Kazak, G. V. Pankina, Y. D. Perfiliev, T. Li, M. Virginie, A. Y. Khodakov, *Catal. Sci. Technol.* **2017**, *7*, 2325–2334.
- [19] D. B. Bukur, D. Mukesh, S. A. Patel, *Ind. Eng. Chem. Res.* **1990**, *29*, 194–204.
- [20] S. K. Das, S. Majhi, P. Mohanty, K. K. Pant, *Fuel Process. Technol.* **2014**, *118*, 82–89.
- [21] H. Kolbel, M. Ralek, *Catal. Rev.* **1980**, *21*, 225–274.
- [22] R. J. O'Brien, B. H. Davis, *Catal. Lett.* **2004**, *94*, 1–6.
- [23] H. Hayakawa, H. Tanaka, K. Fujimoto, *Appl Catal A Gen* **2006**, *310*, 24–30.
- [24] V. R. R. Pendyala, G. Jacobs, H. H. Hamdeh, W. D. Shafer, D. E. Sparks, S. Hopps, B. H. Davis, *Catal. Lett.* **2014**, *144*, 1624–1635.
- [25] S. Li, A. Li, S. Krishnamoorthy, E. Iglesia, *Catal. Lett.* **2001**, *77*, 197–205.
- [26] H. Wan, B. Wu, C. Zhang, H. Xiang, Y. Li, *J Mol Catal A Chem* **2008**, *283*, 33–42.
- [27] K. Pansanga, N. Lohitharn, A. C. Y. Chien, E. Lotero, J. Panpranot, P. Prasertdam, J. G. Goodwin, *Appl Catal A Gen* **2007**, *332*, 130–137.
- [28] C. Zhang, Y. Yang, Z. Tao, T. Li, H. Wan, H. Xiang, Y. Li, *Acta Physico-Chimica Sinica* **2006**, *22*, DOI 10.1016/S1872-1508(06)60064-8.
- [29] L. A. Cano, A. A. Garcia Blanco, G. Lener, S. G. Marchetti, K. Sapag, *Catal. Today* **2017**, *282*, 204–213.



- [30] S. Li, S. Krishnamoorthy, A. Li, G. D. Meitzner, E. Iglesia, *J. Catal.* **2002**, *206*, 202–217.
- [31] W. Ma, E. L. Kugler, D. B. Dadyburjor, *Energy Fuels* **2011**, *25*, 1931–1938.
- [32] W. Gong, R.-P. Ye, J. Ding, T. Wang, X. Shi, C. K. Russell, J. Tang, E. G. Eddings, Y. Zhang, M. Fan, *Appl. Catal. B* **2020**, *278*, 119302.
- [33] H. Wan, B. Wu, C. Zhang, H. Xiang, Y. Li, *J. Mol. Catal. A Chem* **2008**, *283*, 33–42.
- [34] X. Tian, T. Wang, Y. Yang, Y. W. Li, J. Wang, H. Jiao, *J. Phys. Chem. C* **2014**, *118*, 20472–20480.
- [35] O. L. J. Gijzeman, T. J. Vink, O. P. van Pruissen, J. W. Geus, *J. Vac. Sci. Technol. A* **1987**, *5*, 718–721.
- [36] E. De Smit, B. M. Weckhuysen, *Chem. Soc. Rev.* **2008**, *37*, 2758–2781.
- [37] R. L. Espinoza, A. P. Steynberg, B. Jager, A. C. Vosloo, *Appl. Catal. A Gen* **1999**, *186*, 13–26.

---

Manuscript received: March 22, 2024  
Revised manuscript received: June 5, 2024  
Accepted manuscript online: June 10, 2024  
Version of record online: August 6, 2024